THE UNIVERSITY *of* EDINBURGH

Edinburgh Research Explorer

Refraction of nonlinear beams by localized refractive index changes in nematic liquid crystals

Link:
Link to publication record in Edinburgh Research Explorer

Document Version:
Publisher's PDF, also known as Version of record

OPEN ACCESS

Refraction of nonlinear beams by localized refractive index changes in nematic liquid crystals

Gaetano Assanto,[1] Antonmaria A. Minzoni,[2] Noel F. Smyth,[3] and Annette L. Worthy[4]

[1]*Department of Electronic Engineering, NooEL—Nonlinear Optics and OptoElectronics Lab, University of Rome "Roma Tre,"*
Via della Vasca Navale 84, 00146 Rome, Italy

[2]*Department of Mathematics and Mechanics, Fenomenos Nonlineales y Mecánica (FENOMEC), Instituto de Investigacion en Matemáticas*
Aplicadas y Sistemas, Universidad Nacional Autónoma de México, 01000 México D.F., México

[3]*School of Mathematics and Maxwell Institute for Mathematical Sciences, University of Edinburgh, Edinburgh EH9 3JZ, Scotland, UK*

[4]*School of Mathematics and Applied Statistics, University of Wollongong, Northfields Avenue, Wollongong, New South Wales 2522, Australia*

The propagation of solitary waves in nematic liquid crystals in the presence of localized nonuniformities is studied. These nonuniformities can be caused by external electric fields, other light beams, or any other mechanism which results in a modified director orientation in a localized region of the liquid-crystal cell. The net effect is that the solitary wave undergoes refraction and trajectory bending. A general modulation theory for this refraction is developed, and particular cases of circular, elliptical, and rectangular perturbations are considered. The results are found to be in excellent agreement with numerical solutions.

PACS number(s): 42.65.Tg, 42.70.Df, 05.45.Yv

I. INTRODUCTION

The contemporary interest in optical spatial solitons in nonlocal, nonlinear media is witnessed by the number of experiments and numerical studies concerning the generation and control of such self-confined wave packets in various materials, geometries, and regimes. In particular, thermal and reorientational dielectrics have hosted a variety of novel soliton-related phenomena, several of them dealing with the all-optical control of the trajectory of self-trapped beams [1–3]. Specifically, optical spatial solitons in nematic liquid crystals, also known as "nematicons" [4], have been demonstrated to undergo path bending and readdressing under the external action of applied voltages or external illumination, both of them distorting the refractive or uniaxial environment in which the self-confined beam propagates [2,3,5–11]. Nematic liquid crystals, in fact, are liquid uniaxial dielectrics in which the optic axis (or director) corresponds to the main axis of the elongated constituent molecules [12]. The resulting polarization- and propagation-dependent refractive index and birefringent walk-off can therefore be modified via electric-field-driven reorientation or distortion of the director distribution in which the self-trapped wave packet propagates. This very same reorientational mechanism is the basis for efficient self-focusing and generation of nematicons at milli-Watt powers or less [6,13,14].

In the present work, the refraction of the trajectory of a nematicon due to variations in the director orientation caused by localized external electric-field variations will be studied, as, for example, in the experiments reported in [10,11]. An analogous study in which the nematicon trajectory changes due to the effect of an air inclusion in the liquid-crystal cell has been reported [15]. A modulation theory for the nematicon evolution based on suitable trial functions in a Lagrangian formulation of the nematicon equations will be developed to derive equations which explain, in simple terms, the nematicon's trajectory. The specific cases of circular and elliptical external fields, as in Refs. [10,11], and rectangular external fields will be considered. It will be shown that the trajectories as given by the modulation theory are in excellent agreement with full numerical solutions of the nematicon equations. In addition, it will be shown that the nematicon trajectory is largely independent of the beam shape. A major conclusion then is that the beam behavior can be described accurately by an equivalent particle moving in a self-consistent potential. This simple description of a beam's trajectory should be applicable to a wide range of nonlinear guided-beam problems, as has been found for dye-doped liquid crystals [16].

II. BACKGROUND DIRECTOR FIELD

Let us consider a planar cell filled with a nematic liquid crystal [13]. The coordinate z will be taken down the axis of the cell and the (x,y) coordinates will be orthogonal to this direction. A uniform external electric field E_p is applied in the x direction to pretilt the molecular director or optic axis of the effective uniaxial at an angle θ_0 to the z direction in order to overcome the Freédericksz threshold and ease the all-optical reorientation [12,13], that is, the nonlinear response due to the rotation of the director when forced by the coplanar electric field in a light beam. The refractive index in the cell is then made nonuniform by applying an additional external electric field E_b which is nonzero in some domain Ω of the (x,z) plane and uniform in the y direction. For simplicity, E_b will be taken to have the constant value E_0 in Ω. This additional electric field may be due to an applied voltage [2,3,8,9] or another light beam [5–7,10,11]. Its effect is to change the director angle by an amount θ_b from the uniform pretilt θ_0. For the particular case of a light valve [9–11], the nonuniformity was produced by applying an electric field localized in z in the y direction, resulting in a nonuniform refractive index in a corresponding region Ω of the (x,z) plane. It was shown that this localized region Ω can be considered to have been produced by an equivalent external electric field in the x direction, localized in the (x,z) plane. Essentially this equivalent electric field can be thought of as an inverse problem for the refractive index change in the region Ω.

The nondimensional equation governing the resulting director angle perturbation θ_b is then [17,18]

$$\nu \frac{\partial^2 \theta_b}{\partial x^2} + \nu \frac{\partial^2 \theta_b}{\partial z^2} - 2q\theta_b = -2|E_b|^2. \tag{1}$$

The appropriate boundary condition is that θ_b is zero at ∞ with θ_b and its first derivatives being continuous on the boundary of Ω. The parameter q is related to the square of the external uniform pretilting field E_p [17–19], and the parameter ν measures the response of the liquid crystal to the light.

The director equation (1) is a standard elliptic partial differential equation and, in principle, can be solved exactly for a number of separable coordinate systems. However, except for standard, simple coordinates, such as rectangular and polar, these exact solutions will not yield a modulation theory in a simple enough form to be useful. In general, they will be infinite-series solutions and a large number of terms in the series will be required to obtain a faithful representation of the physics. In the present work, we will then use variational approximations in the cases for which there are not simple exact solutions of (1).

Let us consider the exact solution of (1) for an infinite stripe domain Ω. We then consider the electric field E_b to be nonzero in the region $z_1 \leqslant z \leqslant z_2$, taking the constant value E_0 there, so that

$$E_b = \begin{cases} E_0, & z_1 \leqslant z \leqslant z_2, \\ 0, & z < z_1 \quad \text{or} \quad z > z_2. \end{cases} \tag{2}$$

Poisson's equation (1) then has the solution

$$\theta_b = \begin{cases} A_1 e^{\kappa z}, & z < z_1, \\ \frac{E_0^2}{q} - A_2 e^{-\kappa z} - A_3 e^{\kappa z}, & z_1 \leqslant z \leqslant z_2, \\ A_4 e^{-\kappa z}, & z > z_2, \end{cases} \tag{3}$$

where $\kappa = \sqrt{2q/\nu}$ and the constants are

$$A_1 = \frac{E_0^2}{2q}(e^{-\kappa z_1} - e^{-\kappa z_2}), \quad A_2 = \frac{E_0^2}{2q}e^{\kappa z_1},$$
$$A_3 = \frac{E_0^2}{2q}e^{-\kappa z_2}, \quad A_4 = \frac{E_0^2}{2q}(e^{\kappa z_2} - e^{\kappa z_1}), \tag{4}$$

as found in [16,20].

Poisson's equation (1) also has a simple exact solution for a circular region. For a circular region Ω, let us take Ω to be a circle of radius R centered at (X, Z) in the (x, z) plane and the electric field to be a constant E_0 inside this circle, so that

$$E_b = \begin{cases} E_0, & (x - X)^2 + (z - Z)^2 \leqslant R^2, \\ 0 & \text{otherwise.} \end{cases} \tag{5}$$

Poisson's equation (1) then has the solution

$$\theta_b = \begin{cases} \frac{E_0^2}{q}[1 - \kappa R K_1(\kappa R) I_0(\kappa r)], & r \leqslant R, \\ \frac{E_0^2}{q}\kappa R I_1(\kappa R) K_0(\kappa r), & r > R. \end{cases} \tag{6}$$

Here

$$r^2 = (x - X)^2 + (z - Z)^2 \tag{7}$$

and κ is as described previously. I_0, K_0 and I_1, K_1 are the modified Bessel functions of order 0 and 1, respectively.

Laplace's equation $\nabla^2 \varphi = 0$ is separable in elliptical coordinates [21]. Unfortunately, for the inhomogeneous elliptic problem (1), the conformal factor generated by the change to elliptical coordinates prevents a useful closed-form solution [21]. However, the separability of the Laplacian shows that the contour lines of the solution are ellipses confocal to the defect

Ω with a modulated exponential decay along the direction normal to the level lines. With this observation, a variational solution of the director equation (1) can be found for an electric field E_b of the form

$$E_b = \begin{cases} E_0, & \frac{(x-X)^2}{R_a^2} + \frac{(z-Z)^2}{R_b^2} \leqslant 1, \\ 0 & \text{otherwise,} \end{cases} \tag{8}$$

where, as before, E_0 is a constant.

The equation for the director perturbation θ_b is the Euler-Lagrange equation for the Lagrangian,

$$L = \int_{-\infty}^{\infty} \int_{-\infty}^{\infty} \left(-\nu|\nabla\theta_b|^2 - 2q\theta_b^2 + 4\theta_b|E_b|^2 \right) dx\,dz. \tag{9}$$

To construct an appropriate trial function, we observe from the solution (6) for a circular defect that the expansion of I_0 for large nonlocality ν gives a practically constant distribution of θ_b in Ω. We shall assume that the same result holds for an elliptical Ω. As the solution for θ_b in elliptical coordinates has elliptical level lines modulated by exponential decay orthogonal to these lines, we take a trial function of the form

$$\theta_b = \begin{cases} C, & \Gamma \leqslant 1, \\ C\Gamma^{-1/4}e^{-\lambda(\Gamma^{1/2}-1)}, & \Gamma \text{ large} \end{cases} \tag{10}$$

for the variational solution for θ_b, where

$$\Gamma = \frac{(x-X)^2}{R_a^2} + \frac{(z-Z)^2}{R_b^2}. \tag{11}$$

The factor $\Gamma^{-1/4}$ has been added to mimic the asymptotic decay of K_0 for large argument, so that the trial function (10) matches the solution (6) when the ellipse Ω becomes the limit of a circle. Substituting this assumed form for θ_b into the Lagrangian (9) and integrating in x and z from $-\infty$ to ∞ gives the averaged Lagrangian. While this is straightforward in principle, one integral cannot be evaluated exactly as a function of λ. This integral is

$$I = \int_{-\infty}^{\infty} \int_{-\infty}^{\infty} \theta_b^2 \, dx\,dz. \tag{12}$$

In polar coordinates, the equation for the ellipse bounding Ω is

$$r(\theta) = \frac{R_a R_b}{\sqrt{R_b^2 \cos^2\theta + R_a^2 \sin^2\theta}}. \tag{13}$$

In polar coordinates in (x, z), the integral (12) is

$$I = \int_0^{2\pi} \int_0^{r(\theta)} C^2 \rho \, d\rho d\theta + \int_0^{2\pi} \int_{r(\theta)}^{\infty} \theta_b^2 \rho \, d\rho d\theta$$
$$= \pi R_a R_b C^2 + \int_0^{2\pi} \int_{r(\theta)}^{\infty} \theta_b^2 \rho \, d\rho d\theta. \tag{14}$$

We need to assume an appropriate form for θ_b in the transition region between the defect and the region in which the Bessel-function-type solution (10) for large Γ applies. This transition region extends between $r(\theta)$ and $\rho \gg \sqrt{\nu}$. In this range, the decay factor $\Gamma^{-1/4}$ in (10) is close to a constant. We may therefore neglect this decay factor and assume that the trial function (10) behaves exponentially (i.e., with no $\Gamma^{-1/4}$ decay

factor). With these approximations, the second integral in (14) becomes

$$
\int_0^{2\pi}\int_{r(\theta)}^{\infty}\theta_b^2\rho\,d\rho d\theta = \int_0^{2\pi}r^2(\theta)\int_0^{\sqrt{\nu}}e^{-2\lambda(\eta-1)}\eta\,d\eta d\theta
$$
$$
+\int_0^{2\pi}r^{3/2}(\theta)\int_{\sqrt{\nu}}^{\infty}e^{-2\eta}\sqrt{\eta}\,e^{2\lambda}\,d\eta d\theta.
$$
(15)

Thus for large ν, the second integral in (15) is negligible and the first can be extended to infinity. The angular integral can be evaluated exactly when $R_a = R_b$ in terms of the area of the circle. A sufficient approximation is to replace the area of the circle by the area of the ellipse when $R_a \neq R_b$.

We then obtain the averaged Lagrangian from (9) and the trial function (10),

$$
\mathcal{L}(C,\lambda) = \pi C^2\nu\left(\frac{1}{4}+\frac{\lambda}{2}\right)\left(1+\frac{3}{8}\frac{(R_a^2-R_b^2)^2}{(R_aR_b)^3}\right)
$$
$$
+\pi q R_a R_b C^2 + \pi q R_a R_b C^2\left(\frac{1}{4\lambda}+\frac{1}{2}\right)
$$
$$
-2\pi|E_0|^2 R_a R_b C.
$$
(16)

The extremum of $\mathcal{L}$ is obtained by solving the equations $\mathcal{L}_C = \mathcal{L}_\lambda = 0$. In the limit of large ν, we obtain

$$
\lambda = \sqrt{\frac{2qR_aR_b}{\nu}}\left(1+\frac{3}{8}\frac{(R_a^2-R_b^2)^2}{(R_aR_b)^3}\right)^{-1/2}
$$
(17)

and

$$
C = \frac{|E_0|^2 R_a R_b}{Q_1+Q_2},
$$
(18)

where

$$
Q_1 = \frac{\nu}{2}\left(\frac{1}{4}+\frac{\lambda}{2}\right)\left(1+\frac{3}{8}\frac{(R_a^2-R_b^2)^2}{(R_aR_b)^3}\right),
$$
$$
Q_2 = qR_aR_b + 2qR_aR_b\left(\frac{1}{4\lambda^2}+\frac{1}{2\lambda}\right).
$$
(19)

The expression (10) then gives the perturbation of the optic axis due to the elliptical defect.

The final defect region Ω considered in the present work is a rectangle of length $2L_a$ in the x direction and $2L_b$ in the z direction, with the rectangle centered at $(x,z) = (X,Z)$. The solution of the director equation (1) is nontrivial for such a region Ω. A resolution of this difficulty is shown by numerical solutions of (1) for a rectangular Ω. As the nonlocality ν is large [17,18], the solution of the elliptic problem (1) is smoothed near the edges of the rectangle, so that the solution for θ_b has level lines which are ellipses and the resulting director perturbation θ_b closely resembles that for an elliptical region Ω. It is then apparent that the director distribution θ_b for a rectangular Ω can be approximated by the elliptical variational solution (10). The corresponding axes R_a and R_b of the equivalent ellipse need to be determined. This is done by requiring that the area of the equivalent ellipse and the rectangle are the same, so that $R_a = 2L_a/\sqrt{\pi}$ and $R_b = 2L_b/\sqrt{\pi}$.

III. MODULATION EQUATIONS

In nondimensional form, the equations governing the propagation of the nematicon through the liquid crystal with the background director angle variation θ_b and resulting refractive index variation are [17,18,23–25]

$$
i\frac{\partial E_n}{\partial z}+i\Delta\theta_b\frac{\partial E_n}{\partial x}+\frac{1}{2}\nabla^2 E_n + E_n\sin 2(\theta_n+\theta_b)=0,
$$
(20)

$$
\nu\nabla^2\theta_n - q\sin 2\theta_n = -2\cos 2\theta_n|E_n|^2,
$$
(21)

with the Laplacian ∇^2 in the xy plane. Here E_n is the envelope of the electric field of the nematicon and θ_n is the optic axis perturbation due to the nematicon. The parameter $\Delta\theta_b$ is the walk-off, with Δ depending on the pretilt angle. In most experimental situations ν is large, $O(10)$–$O(100)$ [2,17,19], and the nematicon is said to be propagating in the nonlocal [17,18,22]. In this nonlocal regime, the optic axis perturbation due to the nematicon extends far beyond the nematicon waist. In Eqs. (20) and (21), the nonlinear correction to the walk-off, $i\Delta\theta_n E_{nx}$, has been neglected as this term is $O(V\theta_n)$, where both V and θ_n are $O(0.1)$. The major nonlinear contribution comes from the last term in (20). It is extremely difficult to perform any analytical analysis of the full nematicon equations (20) and (21). To enable such analysis, a small-angle assumption is made so that it is assumed that the perturbation θ_n of the director angle from the background value is small. With this assumption, the full nematicon equations (20) and (21) become

$$
i\frac{\partial E_n}{\partial z}+i\Delta\theta_b\frac{\partial E_n}{\partial x}+\frac{1}{2}\nabla^2 E_n + 2E_n(\theta_n+\theta_b)=0,
$$
(22)

$$
\nu\nabla^2\theta_n - 2q\theta_n = -2|E_n|^2,
$$
(23)

on expanding the trigonometric functions to first order in their Taylor series. This small-angle assumption is justified for the low, milli-Watt power levels employed in experiments [2,13]. For the examples considered in this work, the angle θ_n is $O(0.1)$ and is usually in the range 0.05–0.2. The nematicon equations (22) and (23) have the Lagrangian

$$
L = i(E^*E_z - EE_z^*) + i\Delta\theta_b(E^*E_x - EE_x^*) - |\nabla E|^2
$$
$$
+4(\theta_n+\theta_b)|E|^2 - \nu|\nabla\theta_n|^2 - 2q\theta_n^2.
$$
(24)

Here the asterisk superscript denotes the complex conjugate.

To calculate the modulation equations for an evolving nematicon, a functional form for the nematicon usually needs to be taken, common forms being a sech and a Gaussian [26,27]. However, we shall leave the functional form of the nematicon free at this stage and take

$$
E = af(\rho_e)e^{i\sigma+iV(x-\xi)} + ige^{i\sigma+iV(x-\xi)},
$$
$$
\theta_n = \alpha f^2(\rho_n),
$$
(25)

where

$$
\rho_e = \frac{\sqrt{(x-\xi)^2+y^2}}{w}, \qquad \rho_n = \frac{\sqrt{(x-\xi)^2+y^2}}{\beta}.
$$
(26)

The amplitudes a, α, widths w, β, position ξ, velocity V, phase σ, and g are all functions of z. The only assumption on the profile f is that it decays fast enough as ρ_e and ρ_n approach ∞ so that any integrals involved in the calculation of the averaged Lagrangian converge. The first term in the trial function for E is a slowly varying nematicon. The second term represents the low wave-number diffractive radiation which accumulates under the nematicon as it evolves. The existence of this radiation shelf in the case of the nonlinear Schrödinger (NLS) equation has been shown from its inverse-scattering solution [26] and in the case of coupled NLS equations from soliton perturbation theory [28,29]. The physical reason for the existence of this shelf of radiation can be simply deduced from the dispersion relation for the linearized electric-field equation (22). This is $\omega = k^2/2$, giving the group velocity $c_g = k$. Hence low wave-number radiation has low group velocity and so accumulates under the evolving nematicon. This radiation is $\pi/2$ out of phase with the nematicon, the in-phase component resulting in changes in the nematicon amplitude, width, and position [26]. The shelf term g allows mass (optical power) to cycle out of and into the nematicon, so that the nematicon's amplitude oscillates as it evolves [26]. The director response in the trial functions (25) has been assumed to have the profile of $|E|^2$. The reason for this is that it is this term which occurs in a Green's-function solution of the director equation (23). Furthermore, such an assumption has been found to give solutions in excellent agreement with full numerical solutions and experimental results [16,19,20,27].

Substituting the trial functions (25) into the Lagrangian (24) and averaging by integrating in x and y from $-\infty$ to ∞ gives the averaged Lagrangian,

$$
\begin{aligned}
\mathcal{L} = &-2(S_2 a^2 w^2 + \Lambda g^2)\left(\sigma' - V\xi' + \frac{1}{2}V^2\right) \\
&- 2S_1 a w^2 g' + 2S_1 g w^2 a' + 4S_1 a w g w' - S_{22} a^2 \\
&- 4\nu S_{42}\alpha^2 - 2q S_4 \alpha^2 \beta^2 + \frac{2A^2 B^2 \alpha a^2 \beta^2 w^2}{A^2\beta^2 + B^2 w^2} \\
&+ 2S_2 a^2 w^2 (2 - \Delta V) F.
\end{aligned}
\tag{27}
$$

The various integrals S_i and S_{ij} are listed in the Appendix. Taking variations of this averaged Lagrangian with respect to the nematicon parameters gives the modulation (variational) equations,

$$
\frac{d}{dz}(S_2 a^2 w^2 + \Lambda g^2) = 0,
\tag{28}
$$

$$
S_1 \frac{d}{dz} a w^2 = \Lambda g\left(\sigma' - V\xi' + \frac{1}{2}V^2\right),
\tag{29}
$$

$$
S_1 \frac{dg}{dz} = \frac{S_{22}a}{2w^2} - \frac{A^2 B^4 \alpha a \beta^2 w^2}{(A^2\beta^2 + B^2 w^2)^2} + \frac{1}{2}S_2 a w(2 - \Delta V)F_w,
\tag{30}
$$

$$
\begin{aligned}
S_2 &\left(\frac{d\sigma}{dz} - V\frac{d\xi}{dz} + \frac{1}{2}V^2\right) \\
&= -\frac{S_{22}}{w^2} + \frac{A^2 B^2 \alpha \beta^2 (A^2\beta^2 + 2B^2 w^2)}{(A^2\beta^2 + B^2 w^2)^2} \\
&+ S_2(2 - \Delta V)\left(F - \frac{1}{2}w F_w\right),
\end{aligned}
\tag{31}
$$

$$
\frac{d}{dz}(S_2 a^2 w^2 + \Lambda g^2)V = S_2 a^2 w^2(2 - \Delta V)F_\xi,
\tag{32}
$$

$$
\frac{d\xi}{dz} = V + \Delta F,
\tag{33}
$$

plus the algebraic equations,

$$
\alpha = \frac{A^2 B^2 \beta^2 a^2 w^2}{2(A^2\beta^2 + B^2 w^2)(2\nu S_{42} + q S_4 \beta^2)},
\tag{34}
$$

$$
\alpha = \frac{A^2 B^4 a^2 w^4}{q S_4 (A^2\beta^2 + B^2 w^2)^2}.
\tag{35}
$$

These equations govern the evolution of the nematicon in the presence of the refractive index inhomogeneity. The effect of the inhomogeneity on the nematicon, the bending of its trajectory, is encompassed in the term

$$
F = \frac{\int_{-\infty}^{\infty}\int_{-\infty}^{\infty} \theta_b(x,z)f^2(x,y)\,dx\,dy}{\int_{-\infty}^{\infty}\int_{-\infty}^{\infty} f^2(x,y)\,dx\,dy}.
\tag{36}
$$

It is not possible to evaluate the integral in the numerator of F given by (36) exactly. However, since the width of the nematicon beam is much smaller than the scale of the variation of θ_b, which is $O(\nu^{1/2})$, θ_b in the integral in the numerator of (36) can be taken to have its value at the center of the nematicon $x = \xi$. With this approximation,

$$
F(\xi,z) = \theta_b(\xi,z).
\tag{37}
$$

This approximation is exact in the case of a stripe defect Ω, for which θ_b is given by (3), as θ_b is independent of x and $F = \theta_b(z)$. In general, the approximation is valid if the trajectory of the nematicon does not overlap the defect region Ω, which is the case in experiments for finite regions [7,10,11].

As the nematicon evolves, it sheds diffractive radiation in order to evolve to a steady state. The damping effect of this shed radiation on the nematicon equations (28)–(35) will not be included since the amount of radiation shed is negligible over the z distances used in the present work, which are $O(10)$. Radiation loss only becomes significant over z distances of $O(100)$ [27]. Furthermore, the velocity and position evolution are essentially decoupled from the amplitude and width oscillation of the nematicon, with the radiation loss having a much greater effect on the latter and a small effect on the former over medium distances [16,20,30–32].

In addition, the nematicon trajectory is largely independent of the functional form of its profile, as can be seen by examining the modulation equations (28)–(35). The shelf of radiation under the evolving nematicon has small amplitude relative to the beam, so that $|g| \ll a$. Then, on using the mass conservation equation (28), the momentum conservation equation (32) can be approximated by

$$
\frac{dV}{dz} = (2 - \Delta V)F_\xi.
\tag{38}
$$

In this approximation, the trajectory of the nematicon is given solely by (38) and (33). The momentum equation (38) can also be derived by averaging the momentum equation derived using Nöther's theorem based on invariances of the Lagrangian (24) to shifts in x [33,34]. As previously mentioned, losses to shed diffractive radiation can be neglected for propagation distances which are not too long. In the nonlocal limit with

large ν, these losses can be neglected for distances less than $z = O(100)$ in the present nondimensional variables [27]. For large propagation distances, a loss term needs to be added to the mass equation (28) [27], so that the approximation leading to (38) from (32) is then not valid. As shown previously, in the nonlocal limit in which ν is large [17,18], F is independent of a and w and the functional form of the beam $f(\rho)$. The position of the beam thus decouples from the oscillation in its amplitude and width, given by (29) and (30). In this approximation, the trajectory of the beam is given solely by the simple system (33) and (38) in which $f(\rho)$ does not appear. A similar decoupling of the amplitude and position evolutions and the independence of the nematicon trajectory from its profile has been found in previous work on the interaction of nematicons with localized refractive index changes [16].

IV. COMPARISON WITH NUMERICAL SOLUTIONS

The full nematicon equations (20) and (21) were solved numerically using the pseudospectral method of Fornberg and Whitham [35], while the modulation equations (28)–(35) were solved using the standard fourth-order Runge-Kutta scheme. The trajectories of the nematicon as given by the numerical and modulation solutions will now be compared.

Let us first consider the case of a nematicon being refracted by a circular region Ω. A comparison between the trajectories as given by the full numerical solution and the solution of the modulation equations is shown in Fig. 1. To within graphical accuracy, there is no difference between the trajectory as given by the full modulation equations (28)–(35) and the momentum approximations (33) and (38). The comparison is excellent with near perfect agreement. It can be seen that the numerical trajectory shows some oscillation after its turning point, while the modulation trajectory does not. The averaging process of modulation theory treats the nematicon as a point particle.
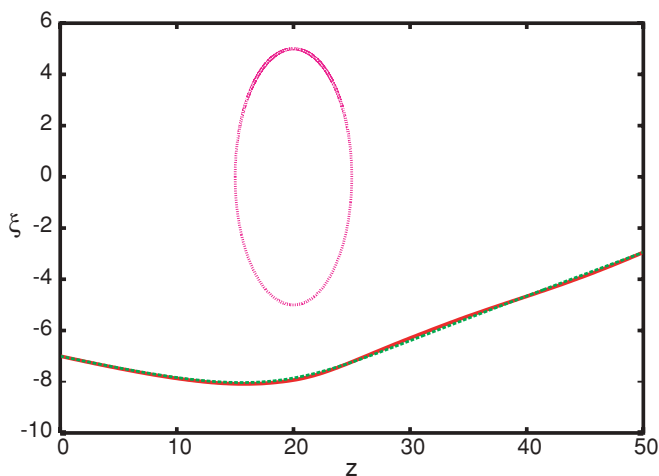
FIG. 1. (Color online) Comparison of nematicon trajectories for a circular region Ω. Numerical solution, — (red); solution of modulation equations, $---$ (green). The initial condition is $f(\rho) = \mathrm{sech}\,\rho$, $a = 2.5$, $w = 2.0$, $V = -0.1$, and $\xi = -7.0$ with $\nu = 200$, $q = 2$, and $\Delta = 1.0$. The defect parameters are $E_0 = 1$, $X = 0$, $Z = 20$, and $R = 5$. The boundary of Ω is given by the dotted (pink) line.
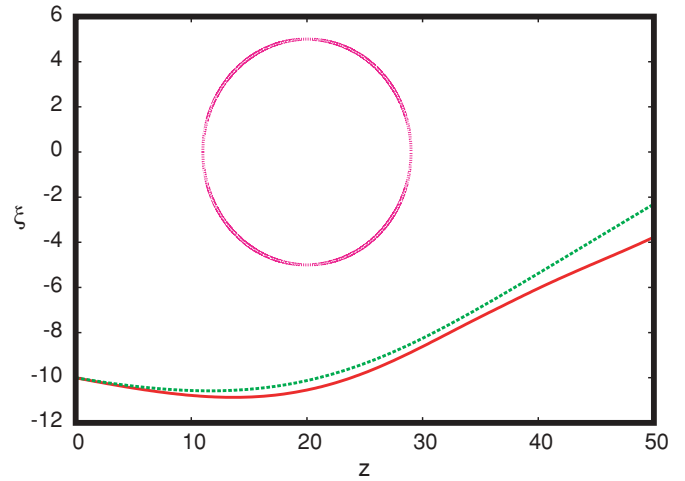
FIG. 2. (Color online) Comparison of nematicon trajectories for an elliptical region Ω. Numerical solution, — (red); solution of modulation equations, $---$ (green). The initial condition is $f(\rho) = \mathrm{sech}\,\rho$, $a = 2.5$, $w = 2.0$, $V = -0.1$, and $\xi = -10.0$ with $\nu = 200$, $q = 2$, and $\Delta = 1.0$. The defect parameters are $E_0 = 1$, $X = 0$, $Z = 20$, and $R_a = 5$, $R_b = 9$. The boundary of Ω is given by the dotted (pink) line.

However, a nematicon has a finite width, so that its tail overlaps the defect Ω. This overlap causes an asymmetry in the nematicon, so that its peak starts to oscillate in position, transverse to its trajectory. The numerical scheme determines the position of the nematicon by the position of its peak. As the nematicon is launched closer to the defect Ω, the oscillation in its trajectory grows due to the increased portion of it in Ω. These oscillations die as the nematicon propagates away from Ω.

Figure 2 shows a similar comparison for an elliptical defect region Ω. The comparison between the trajectories as given by the numerical and modulation solutions is not as close as for the circular Ω, but it is still good. Again, the full modulation equations (28)–(35) and the momentum approximations (33) and (38) give the same trajectories to graphical accuracy. The reason the comparison is not as good as for a circular Ω is that the solution for the director distribution θ_b is not an exact solution as it is for the circular Ω, and this introduces errors in the modulation equations. The numerical trajectory again shows an oscillation due to the overlap of the nematicon with the region Ω.

The final defect geometry considered is a rectangular region Ω. A limiting case of a rectangle is an infinite stripe in the x direction. A trajectory comparison for this limiting case is shown in Fig. 3, for which there is perfect agreement between the numerical and modulation solutions, with the momentum approximations (33) and (38) giving identical results to the full modulation equations to graphical accuracy. As for the circle, this perfect agreement is due to there being an exact solution for the director perturbation θ_b. In the case of an infinite stripe, $F = \theta_b(z)$ and so it does not depend on the nematicon position ξ. It can then be seen from the momentum equations (32) and (38) that momentum is conserved, so that the nematicon trajectory returns to its initial direction after leaving the stripe, as seen in the figure. The numerical nematicon trajectory does not show the same oscillations as for the finite defects as
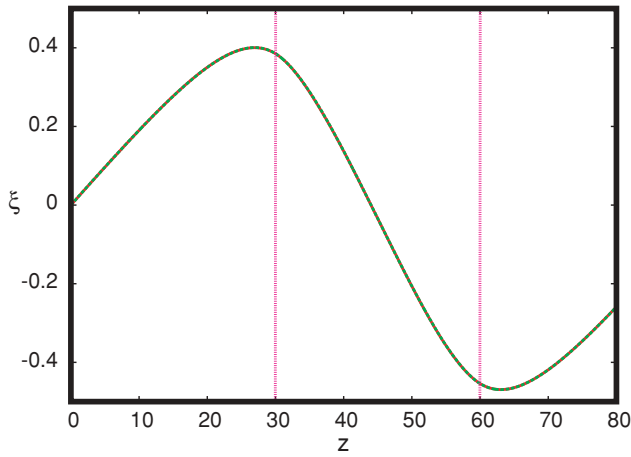
FIG. 3. (Color online) Comparison of nematicon trajectories for a stripe region Ω. Numerical solution, — (red); solution of modulation equations, – – – (green). The initial condition is $f(\rho) = \operatorname{sech} \rho$, $a = 1.5$, $w = 3.5$, $V = 0.02$, and $\xi = 0.0$ with $\nu = 200$, $q = 2$, and $\Delta = 0.5$. The defect parameters are $E_0 = 0.5$, $z_1 = 30$, and $z_2 = 60$. The boundary of Ω is given by the dotted (pink) lines.

the entire nematicon enters the defect region Ω. This case of an infinite stripe generating a director angle perturbation is essentially the same case as considered in [16,20], for which the director perturbation was generated by an illumination beam in the x direction. The main difference is that this work took into account the decay of the illumination beam due to scattering losses, which meant that momentum was not conserved and the nematicon did not return to its initial propagation direction on exiting the illumination region.

Let us now consider the effect on the trajectory of a nematicon of a finite rectangular region Ω. A comparison is shown in Fig. 4. The agreement of the trajectory as predicted by the modulation equations with the numerical trajectory is
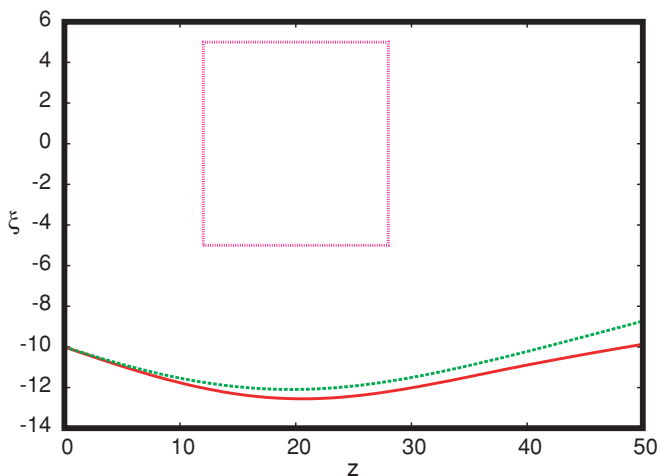
very good, with the level of agreement similar to that for the elliptical region shown in Fig. 2. Again the momentum approximation and the full modulation equations give the same result to graphical accuracy. This level of agreement between the modulation and numerical solutions is expected as the director perturbation angle θ_b is again found as an approximate solution, not an exact solution, of the director equation (1), as is the case for the elliptical region Ω. The numerical trajectory again shows a slight oscillation, for the same reason as for the circular and elliptical defects Ω.

Previous work on the propagation of a nematicon through an infinite stripe defect, as in Fig. 3, found that the trajectory of the nematicon is independent of the functional form of its profile [16], as discussed in the previous section. As there is no known exact solution for the steady nematicon, this greatly adds to the modulation theory approach used here as it is based on using a reasonable approximation for this nematicon profile, as in (25). The discussion leading to the momentum equation (38) would suggest that the nematicon trajectory is
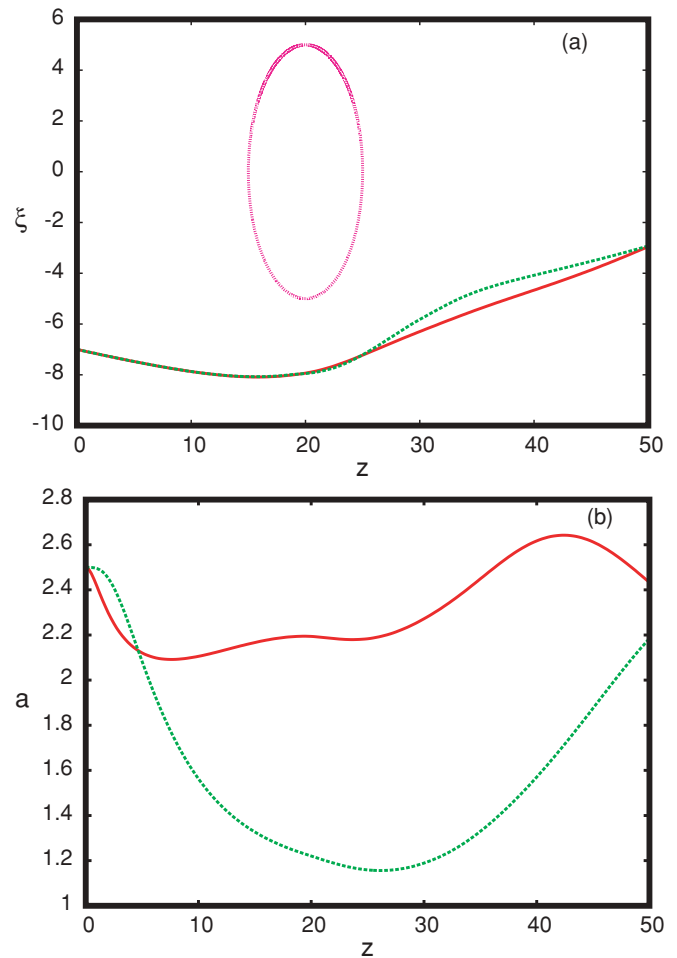

FIG. 5. (Color online) Comparison of nematicon trajectories for a circular region Ω. Numerical solution for a sech input beam $f(\rho) = \operatorname{sech} \rho$, — (red); numerical solution for a Gaussian input beam $f(\rho) = \exp(-\rho^2)$, – – – (green). The initial condition is $a = 2.5$, $w = 2.0$ for the sech and $a = 2.5$, $w = 3.0$ for the Gaussian with $V = -0.1$, $\xi = -7.0$, $\nu = 200$, $q = 2$, and $\Delta = 1.0$. The defect parameters are $E_0 = 1$, $X = 0$, $Z = 20$, and $R = 5$. The boundary of Ω is given by the dotted (pink) line. Part (a) trajectory and part (b) amplitude.

FIG. 4. (Color online) Comparison of nematicon trajectories for a rectangular region Ω. Numerical solution, — (red); solution of modulation equations, – – – (green). The initial condition is $f(\rho) = \operatorname{sech} \rho$, $a = 2.5$, $w = 2.0$, $V = -0.2$, and $\xi = -10.0$ with $\nu = 200$, $q = 2$, and $\Delta = 1.0$. The defect parameters are $E_0 = 1$, $X = 0$, $Z = 20$, $R_a = 5$, and $R_b = 8$. The boundary of Ω is given by the dotted (pink) line.

again independent of its profile for the localized refractive index changes considered here. However, while this is true for the modulation equations, the localized nature of Ω leads to an effect not accounted for in the modulation theory. A comparison between the nematicon trajectories for a sech and a Gaussian input for a circular region Ω is shown in Fig. 5. While the initial amplitudes are the same, the initial width of the Gaussian beam was increased to 3 from the width 2 of the sech beam as the faster decay rate of the Gaussian beam means that it needs a larger width so that its mass is above the threshold for a nematicon to form. However, for these initial parameters, the half-widths of the two beams are nearly the same. It can been seen that the trajectories are identical until the turning point is reached. After this point, the Gaussian beam shows more oscillation in its position than the sech beam. The reason for this can be seen from the amplitude evolution shown in Fig. 5(b). The Gaussian beam shows a greater decrease in amplitude, and thus an increase in width, which means that more of the beam intrudes into the defect region Ω, leading to the greater oscillation in its trajectory. This reinforces the effect of the finite size of a nematicon. The modulation theory of Sec. III treats the nematicon as a point particle and so it cannot account for its distortion due to its overlap with the region Ω. This is especially the case as the interaction of the nematicon with the defect region is contained in the interaction term F given by (36). This interaction term has been approximated to (37), which only accounts for the refractive index around the peak of the nematicon.

V. CONCLUSIONS

The evolution of the trajectory of a nematicon in nematic liquid crystals due to localized variations in the director orientation (refractive index) caused by external effects, such as other optical beams or a static electric field, has been investigated. This study was carried out in the limit in which the reorientation of the director due to the nematicon is smaller than that due to the localized defect, so that the director reorientation caused by the defect can be decoupled from that caused by the nematicon. A modulation theory based on using trial functions in an averaged Lagrangian formulation was developed, and excellent agreement with full numerical solutions was found for the nematicon trajectory in a variety of defect configurations. It was found that the nematicon trajectory was nearly independent of the profile of the nematicon. In the limit of an infinite stripe defect, the trajectory is fully independent of the profile, as has been found previously [16]. For a finite defect, the beam trajectory is affected by the overlap of the beam with the defect region, with this overlap inducing an asymmetry in the nematicon profile and a consequent oscillation in its trajectory. The closer the nematicon is to the defect, the greater is this oscillation and the more the trajectory depends on the beam profile. The weak dependence of the beam trajectory on its profile is a great advantage for modulation theories because these need to assume a profile as there is no exact solution of the nematicon equations for a steady nematicon.

We remark that similar results to those obtained here could be found for the propagation of a vortex rather than the present solitary wave beam, provided the electric-field-induced defect does not destabilize the vortex. The analysis of Minzoni *et al.* [36] for a vortex in a circular cell could be extended to study the effect of localized defects as in the present work.

Finally, we remark on three-space-dimensional beam propagation. In this three-dimensional case, the director distribution θ_b due to the defect field E_b will be computed numerically by solving the equivalent of (1), with this numerical solution used in the modulation equations for the nematicon propagation. This will provide an efficient method for solving high-dimensional beam propagation problems.

APPENDIX: INTEGRALS

The integrals S_i and $S_{i,j}$ in the modulation equations are

$$S_1 = \int_0^\infty \rho f(\rho)\, d\rho, \quad S_2 = \int_0^\infty \rho f^2(\rho)\, d\rho,$$

$$S_{22} = \int_0^\infty \rho \left(\frac{df}{d\rho}\right)^2 d\rho, \quad S_{x32} = \int_0^\infty \rho^3 f^2(\rho)\, d\rho, \quad \text{(A1)}$$

$$S_{42} = \frac{1}{4}\int_0^\infty \rho \left(\frac{d}{d\rho} f^2(\rho)\right)^2 d\rho, \quad S_4 = \int_0^\infty \rho f^4(\rho)\, d\rho.$$

For $f(\rho) = \operatorname{sech}\rho$,

$$S_1 = 2C, \quad S_2 = \ln 2, \quad S_{22} = \tfrac{1}{3}\ln 2 + \tfrac{1}{6},$$

$$S_{x32} = 1.352\,314\,016\ldots, \quad S_{42} = \tfrac{2}{15}\ln 2 + \tfrac{1}{60}, \quad \text{(A2)}$$

$$S_4 = \tfrac{2}{3}\ln 2 - \tfrac{1}{6}.$$

Here C is the Catalan constant $C = 0.915\,965\,594\ldots$ [21]. For $f(\rho) = \exp(-\rho^2)$

$$S_1 = \tfrac{1}{2}, \quad S_2 = \tfrac{1}{4}, \quad S_{22} = \tfrac{1}{2}, \quad S_{x32} = \tfrac{1}{8},$$

$$S_{42} = \tfrac{1}{8}, \quad S_4 = \tfrac{1}{8}. \quad \text{(A3)}$$

The constants A and B arising in the modulation equations are

$$A = \frac{S_2 \sqrt{2}}{\sqrt{S_{x32}}} \quad \text{and} \quad B = \sqrt{2S_2}. \quad \text{(A4)}$$

[1] C. Rothschild, B. Alfassi, O. Cohen, and M. Segev, Nat. Phys. **2**, 769 (2006).

[2] M. Peccianti, C. Conti, G. Assanto, A. De Luca, and C. Umeton, Nature **432**, 733 (2004).

[3] M. Peccianti, A. Dyadyusha, M. Kaczmarek, and G. Assanto, Nat. Phys. **2**, 737 (2006).

[4] G. Assanto, M. Peccianti, and C. Conti, Opt. Photon. News **14**, 44 (2003).

[5] A. Pasquazi, A. Alberucci, M. Peccianti, and G. Assanto, Appl. Phys. Lett. **87**, 261104 (2005).

[6] S. V. Serak, N. V. Tabiryan, M. Peccianti, and G. Assanto, IEEE Photonics Technol. Lett. **18**, 1287 (2006).

[7] A. Piccardi, G. Assanto, L. Lucchetti, and F. Simoni, Appl. Phys. Lett. **93**, 171104 (2008).

[8] A. Piccardi, M. Peccianti, G. Assanto, A. Dyadyusha, and M. Kaczmarek, Appl. Phys. Lett. **94**, 091106 (2009).

[9] A. Alberucci, A. Piccardi, U. Bortolozzo, S. Residori, and G. Assanto, Opt. Lett. **35**, 390 (2010).

[10] A. Piccardi, A. Alberucci, U. Bortolozzo, S. Residori, and G. Assanto, Appl. Phys. Lett. **96**, 071104 (2010).

[11] A. Piccardi, A. Alberucci, U. Bortolozzo, S. Residori, and G. Assanto, IEEE Photonics Technol. Lett. **22**, 694 (2010)

[12] I. C. Khoo and N. T. Wu, *Optics and Nonlinear Optics of Liquid Crystals* (World Scientific Publ., Singapore, 1993).

[13] M. Peccianti, G. Assanto, A. De Luca, C. Umeton, and I. C. Khoo, Appl. Phys. Lett. **77**, 7 (2000).

[14] A. Piccardi, A. Alberucci, and G. Assanto, Electron. Lett. **46**, 790 (2010).

[15] Y. V. Izdebskaya, V. G. Shvedov, A. S. Desyatnikov, W. Krolikowski, and Y. S. Kivshar, Opt. Lett. **35**, 1692 (2010).

[16] G. Assanto, B. D. Skuse, and N. F. Smyth, Phys. Rev. A **81**, 063811 (2010).

[17] C. Conti, M. Peccianti, and G. Assanto, Phys. Rev. Lett. **91**, 073901 (2003).

[18] C. Conti, M. Peccianti, and G. Assanto, Phys. Rev. Lett. **92**, 113902 (2004).

[19] G. Assanto, A. A. Minzoni, M. Peccianti, and N. F. Smyth, Phys. Rev. A **79**, 033837 (2009).

[20] G. Assanto, B. D. Skuse, and N. F. Smyth, Photon. Lett. Poland **1**, 154 (2009).

[21] M. Abramowitz and I. A. Stegun, *Handbook of Mathematical Functions with Formulas, Graphs and Mathematical Tables* (Dover Publications, Inc., New York, 1972).

[22] M. Peccianti, K. A. Brzdakiewicz, and G. Assanto, Opt. Lett. **27**, 1460 (2002).

[23] M. Peccianti, A. Fratalocchi, and G. Assanto, Opt. Express **12**, 6524 (2004).

[24] C. García-Reimbert, A. A. Minzoni, and N. F. Smyth, J. Opt. Soc. Am. B **23**, 294 (2006).

[25] C. García-Reimbert, A. A. Minzoni, N. F. Smyth, and A. L. Worthy, J. Opt. Soc. Am. B **23**, 2551 (2006).

[26] W. L. Kath and N. F. Smyth, Phys. Rev. E **51**, 1484 (1995).

[27] A. A. Minzoni, N. F. Smyth, and A. L. Worthy, J. Opt. Soc. Am. B **24**, 1549 (2007).

[28] J. Yang, Stud. Appl. Math. **98**, 61 (1997).

[29] D. E. Pelinovsky and Y. Yang, Stud. Appl. Math. **105**, 245 (2000).

[30] C. García-Reimbert, A. A. Minzoni, T. R. Marchant, N. F. Smyth, and A. L. Worthy, Physica D **237**, 1088 (2008).

[31] B. D. Skuse and N. F. Smyth, Phys. Rev. A **77**, 013817 (2008).

[32] B. D. Skuse and N. F. Smyth, Phys. Rev. A **79**, 063806 (2009).

[33] I. M. Gelfand and S. V. Fomin, *Calculus of Variations* (Prentice-Hall, Inc., Englewood Cliffs, N. J., 1963).

[34] D. J. Kaup and A. C. Newell, Proc. R. Soc. London A **361**, 413 (1978).

[35] B. Fornberg and G. B. Whitham, Philos. Trans. R. Soc. London A **289**, 373 (1978).

[36] A. A. Minzoni, N. F. Smyth, and Z. Xu, Phys. Rev. A **81**, 033816 (2010).